On the Realizability of Strongly Divergent Supergradient Flows

JULIA NOGUES PAEGLE AND JAN PAEGLE

Department of Meteorology, University of Utah, Salt Lake City 84112

(Manuscript received 19 March 1976, in revised form 9 August 1976)

ABSTRACT

Time-dependent flow solutions for steady supergradient pressure patterns are presented for a variety of initial flow configurations. These solutions discriminate initial conditions and pressure patterns that produce stable and unstable flow evolutions. It is shown that steady-state divergent flows are realizable for commonly observed pressure patterns of the upper troposphere. In these cases, the steady state is approached on relatively short time scales. Solutions agree roughly with observed features of atmospheric flows and constitute a plausible explanation for strong upper level outflows.

1. Introduction

There are two unique features of synoptic scale upper tropospheric motions in the tropical atmosphere. These are the strongly divergent flows that are associated with the upper branch of the Hadley circulation (Sadler, 1975; Krishnamurti, 1971) and the high frequency of supergradient high pressure region (Ellsaesser, 1968; Paegle and Paegle, 1976). Both phenomena appear to be quasi-steady state elements of the tropical climate; and it is reasonable to suppose that their correct simulation could be important for global numerical weather prediction.

There are relatively few mechanisms that may permit divergence for steady state flows. One of these may be internal friction as hypothesized by Holton and Colton (1972) and Lindzen (1974). This hypothesis holds that mixing of cyclonic low level vorticity into anticyclonic upper tropospheric circulation may be sufficient to explain the divergence and vorticity fields.

In Section 3 we present evidence indicating that the rotating outflow from cumulonimbus anvils may not be strongly dependent upon low level vorticity. If this is generally true, then vorticity mixing may not be the only important mechanism driving such divergence.

In Section 4 we suggest that strong high pressure areas may be partly responsible for large scale upper outflows in the tropics. These upper high pressure centers seem to be particularly noticeable in warm core disturbances that are characterized by strong convection (MacDonald, 1976).

We speculated upon these points in earlier papers (Paegle and Paegle, 1974, 1976) which presented steady state divergent solutions for strong high pressure fields. The balance equation is non-elliptic for such pressure patterns. Since there is no solenoidal gradient wind solution in these cases, we refer to the resulting flow as "supergradient" (not to be confused with the anomalous solution of the gradient wind equations). A major purpose of the present paper is to point out the rapid convergence of transient flow solutions to the steady state solutions which are thereby shown to be realizable for a wide variety of commonly observed supergradient pressure patterns.

The solution convergence rate depends directly upon the strength of the high pressure pattern and upon the nonlinearity of the mathematical model. Analytic studies of mutual adjustment of wind and pressure patterns have been extensively done (see Blumen, 1972, for a review). However, few of these study the nonlinear problems and these investigate only weakly nonlinear cases or rather special flow types.

We simplify the mathematical problem in Section 2 to focus upon the adjustment of the horizontal wind to a given time invariant supergradient pressure field. The pressure field may be assumed to be maintained by low level mass inflow and heating in warm core disturbances, but neither process is explicitly modelled in our analysis. Partial justification for this approach is provided by the fact that, for synoptic scales, the strong high pressure patterns that are modelled apparently persist on time scales longer than one day (MacDonald, 1976; Paegle and Paegle, 1976), while the flow adjustment toward a steady state does not require mass adjustment and is predicted to occur in less than a day (Section 4). On mesoscales, available data implies that the flow adjustment scale is similar to time scales of mesoscale pressure patterns (Section 3).

A benefit of this analysis is that strong nonlinearities and arbitrary initial kinematic configurations may be locally included. The time scales of adjustment as

well as the relevant physical processes are easily described.

2. Mathematical analysis

a. Assumptions

The analysis is based upon the divergence, vorticity, and deformation equations in Cartesian coordinates. Neglecting terms arising from the earth's sphericity as well as tilting terms associated with horizontal variation of vertical motion, these equations are

$$\frac{dD}{dt}=\tfrac{1}{2}[\eta^2-(A^2+B^2+D^2)]-\left(\nabla^2\phi+\frac{f^2}{2}\right), \tag{1}$$

$$\frac{dA}{dt}=-DA+f(B-B_g), \tag{2}$$

$$\frac{dB}{dt}=-DB-f(A-A_g), \tag{3}$$

$$\frac{d\eta}{dt}=-\eta D, \tag{4}$$

where $D=u_x+v_y$, $A=v_x+u_y$, $B=v_y-u_x$, $\eta=v_x-u_y+f$; the Coriolis parameter f is taken as constant; $A_g=f^{-1}(\phi_{xx}-\phi_{yy})$, $B_g=2f^{-1}\phi_{xy}$; and ϕ is the geopotential.

We consider force fields such that $\nabla^2\phi<-f^2/2$ (non-elliptic for the balance equation) and this as well as A_g and B_g constant in space and time. We define γ such that $\gamma^2/2=-(\nabla^2\phi+f^2/2)$. This quantity is a measure of the non-ellipticity of the pressure field (Paegle and Paegle, 1974).

Eqs. (1) through (4) then describe the evolution of the kinematic field in the vicinity of a supergradient high pressure area. Its solution may be viewed as time variations of A, B, D and η following trajectories (Lagrangian coordinates) or can be considered to give the local time changes if advective effects are negligible. The major assumptions are omission of thermodynamics; tilting terms and constancy of $\nabla^2\phi$, A_g and B_g. These are similar to assumptions frequently invoked in nonlinear transient Ekman layer studies (Greenspan, 1968). However, our assumption of time invariant pressure throughout the fluid is stronger than the usual assumption of time invariant pressure field at infinity. In our case viscosity is not required to reach steady state.

We first consider a circular anticyclonic pressure field such that $A_g=B_g=0$. Eqs. (2), (3) and (4) can then be combined to obtain the time invariant quantity $(A^2+B^2)/\eta^2=(A_0^2+B_0^2)/\eta_0^2$ where the subscript 0 refers to the initial state.

Then (1) through (4) reduce to

$$\frac{dD}{dt}=\tfrac{1}{2}(b\eta^2-D^2)+\tfrac{1}{2}\gamma^2, \tag{5}$$

$$\frac{d\eta}{dt}=-\eta D, \tag{6}$$

where $b=1-(A_0^2+B_0^2)/\eta_0^2$.

b. Integral curves

Two basically different types of solution are distinguished by

(i) $b=\beta^2>0$,

(ii) $b=-\beta^2<0$,

which correspond to cases with weak and strong initial deformation, respectively. We obtain:

$$\text{for (i)}\quad \frac{dD}{d\eta}=\frac{\tfrac{1}{2}(\beta^2\eta^2-D^2)+\tfrac{1}{2}\gamma^2}{-\eta D} \tag{7}$$

$$\text{for (ii)}\quad \frac{dD}{d\eta}=\frac{-\tfrac{1}{2}(\beta^2\eta^2+D^2)+\tfrac{1}{2}\gamma^2}{-\eta D}. \tag{8}$$

Integral curves in (η,D) space can be easily obtained from these equations. For case (i) they are all of the form

$$(\eta\pm C)^2+\frac{D^2}{\beta^2}=r^2. \tag{9}$$

Here C and r are obtained from the conditions

$$\left.\begin{aligned} C^2+\frac{\gamma^2}{\beta^2}&=r^2\\ (\eta_0\pm C)^2+\frac{D_0^2}{\beta^2}&=r^2\end{aligned}\right\}.$$

For case (ii) the corresponding curves are given by

$$(\eta\pm C)^2-\frac{D^2}{\beta^2}=\pm r^2, \tag{10}$$

with C and r obtained from

$$\left.\begin{aligned} C^2-\frac{\gamma^2}{\beta^2}&=\pm r^2\\ (\eta_0\pm C)^2-\frac{D_0^2}{\beta^2}&=\pm r^2\end{aligned}\right\}.$$

The sign on the right-hand side of these equations is determined according to $C^2-\gamma^2/\beta^2\gtrless 0$. Eqs. (9) and (10) give the other time invariants required to

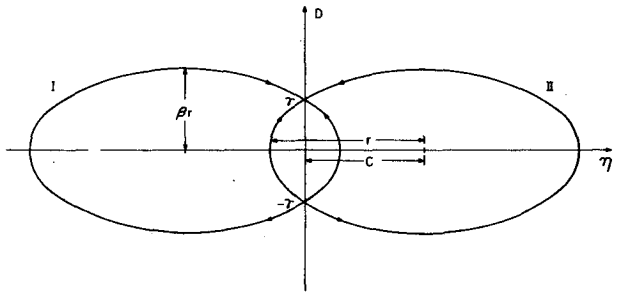

FIG. 1. Integral curves for case of weak initial deformation. Symbols defined in text.

obtain the transient solution. For a complete description of the integral curves it is necessary to isolate the singular points in (D,η) space. Eq. (7) shows that there are only two singular points for case (i) at $\eta=0$, $D=\pm\gamma$. A Taylor expansion in the neighborhood of these points (Davies and James, 1966) reveals that the point $\eta=0$; $D=\gamma$ is stable; while $\eta=0$; $D=-\gamma$ is unstable. This means that, for increasing time, points in the neighborhood of the stable or unstable point move into or away from the respective point. This analysis also indicates that the distance from the stable singularity decreases as $e^{-\gamma t}$ for points close to the singular point implying an adjustment time scale of $1/\gamma$.

Fig. 1 depicts one set of integral curves for the case of weak initial deformation. All integral curves pass through $\eta=0$; $D=\gamma$; therefore all possible trajectories in this phase space converge to this point. This clearly indicates that any arbitrarily selected initial condition will evolve to the steady state represented by $\eta=0$; $D=\gamma$. The trajectories decelerate as they approach the stable singularity and it would take an infinitely long time to reach this point. Nevertheless, as will be shown in subsequent sections; the solution approaches the steady state value in relatively short times.

Eq. (8) has four singularities. They are listed in Table 1 and classified according to their stability characteristics. Fig. 2 shows integral curves obtained from (10). The domains which contain initial states leading toward steady state flow are hatched. These domains include the most commonly observed synoptic scale flows. The unstable domain implies rather large rotation and/or convergence in the presence of a strong circular high pressure cell.

TABLE 1. Classification of singularities for cases of strong initial deformation.

D	η	Singularity
γ	0	stable
$-\gamma$	0	unstable
0	$\pm\gamma/\beta$	unstable (col)

c. Stability analysis including geostrophic deformation

Steady state solutions for (1)–(4) are

$$\eta=0,$$

$$D=D_s=\left(\gamma^2-\frac{A_g^2+B_g^2}{1+D_s^2/f^2}\right)^{\frac{1}{2}},$$

$$A=A_s=\frac{A_g-(D_s/f)B_g}{1+D_s^2/f^2},$$

$$B=B_s=\frac{B_g+(D_s/f)A_g}{1+D_s^2/f^2}.$$

Defining new variables $x=D-D_s$, $y=B-B_s$ and $z=A-A_s$, equations similar to (1)–(4) can be obtained for x, y, z, η. Expanding the right-hand side of these in a Taylor series about the origin they become

$$\frac{dx}{dt}=-D_sx-B_sy-A_sz, \tag{11}$$

$$\frac{dy}{dt}=-B_sx-D_sy-fz, \tag{12}$$

$$\frac{dz}{dt}=-A_sx+fy-D_sz, \tag{13}$$

$$\frac{d\eta}{dt}=-D_s\eta. \tag{14}$$

For exponential solutions of the form $e^{\lambda t}$, the eigenvalues are found to be

$$\lambda_{1,2}=-D_s,$$
$$\lambda_{3,4}=-D_s\pm i[f^2-(A_s^2+B_s^2)]^{\frac{1}{2}}.$$

Therefore, the real part of the solution always contains functions that decay exponentially with time, indicating that points in the neighborhood of the steady state would evolve into it on time scales $1/\gamma$. The only exception is for the case that $A_s^2+B_s^2>f^2$ and $(A_s^2+B_s^2-f^2)^{\frac{1}{2}}>D_s$. These are rather extreme conditions for synoptic scale flows.

Due to the complexity of these equations only the linearized stability analysis is described in this case of non-zero geostrophic deformation. Subsequent sections discuss particular time evolution for various scales of observed supergradient pressure fields.

3. Application to small scales

In this section we present implications of the above analysis to upper outflow of local convectively disturbed regions. Conclusions are tentative, since it is not possible to separate geopotential data observation errors from actual small scale variability and there

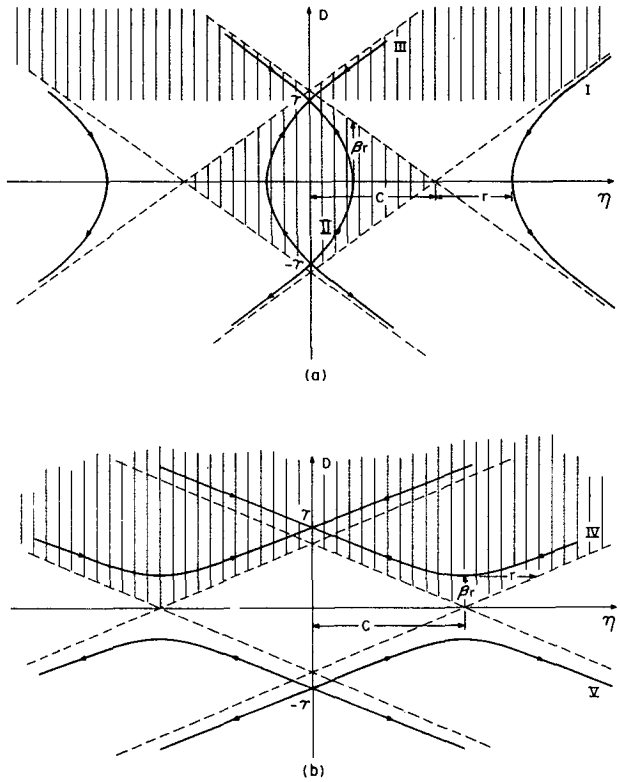

FIG. 2. Integral curves for case of strong initial deformation. (a) corresponds to a case for which $C^2-\gamma^2/\beta^2>0$ and (b) for $C^2-\gamma^2/\beta^2<0$. Significance of hatched regions and symbols is discussed in text.

are only a few data studies that derive reliable geopotential fields for these scales.

a. *Mid-latitude squall line*

Fankhauser (1974) analyzed mesonet wind data in the vicinity of a mid-latitude squall line. All terms of the divergence equation were evaluated directly, except the geopotential term which was found as a residual. The horizontal resolution was on the order of 40 km, about the scale of a large thunderstorm. Using his data at outflow levels the peak value of 0.9×10^{-3} s^{-1} may be computed for γ. This suggests an adjustment time scale on the order of 20 min toward a steady state divergence of 0.9×10^{-3} s^{-1} at the same point. This agrees roughly with the observed value of the divergence of 0.6×10^{-3} s^{-1} and the observation that the local time derivative of the divergence is about one third of the D^2 and geopotential terms in the divergence equation, and the other nonlinear terms (vorticity, deformation, and tilting terms) are at least an order of magnitude smaller than the divergence term.

Fankhauser's results also indicate that advective terms are important just below and above the level of maximum divergence. However, at this particular level the exponentially decaying solution of the previous section agrees well with data when initial conditions are taken 50 mb lower and 20 min earlier (consistent with Fankhauser's analyzed vertical motion fields), and if small geostrophic deformation ($A_0^2+B_0^2<f^2$) is assumed. This comparison indicates that the simple model of the last section (applied in a linearized and Lagrangian sense) is capable of describing such observations.

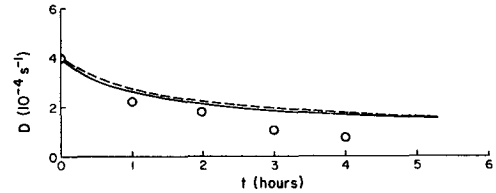

FIG. 3. Time evolution of divergence. Solid and dashed lines are model predictions using initial values for η_0 of -7.5×10^{-5} s^{-1} and 1.4×10^{-4} s^{-1}, respectively. For both cases $\gamma=1.5\times10^{-4}$ s^{-1} and $D_0=4\times10^{-4}$ s^{-1}. Circles are observations taken from Chang (1974).

b. *Tropical mesoscale cloud cluster*

Chang (1974) used the anvil spread rate above a subtropical mesoscale disturbance analyzed through ATS satellite images to deduce outflow from convective regions. The associated geopotential fields were computed by using the hydrostatic equation and an anvil "overshooting" estimate. Thus the motion and mass field were evaluated independently. The time behavior of the observed divergence and vorticity fields is shown in Figs. 3 and 4.

From Fig. 5 of Chang (1974) (reproduced as Fig. 5 here) we estimate a value of 1.5×10^{-4} s^{-1} for γ in the convective area of concern (area A) and assume zero geostrophic and initial deformation ($\beta=1$). Locally, a larger value of γ may be justified as in the finer scale analysis of Fankhauser (1974) and on a larger scale a smaller value would result. However, the chosen value appears to be a reasonable compromise for the 300 km radius of the 200 mb high pressure pattern associated with the disturbance.

The transient behavior of ρ and D for the case of weak initial deformation can be obtained by integration of (5) and (6) using invariant (9) (see Appendix).

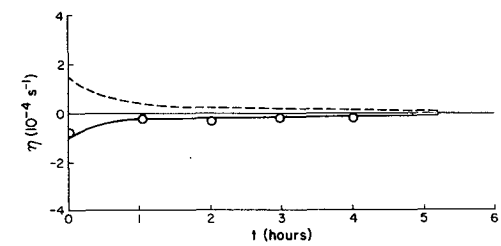

FIG. 4. Same as Fig. 3 for absolute vorticity. Circles are observations obtained from Chang (1974).

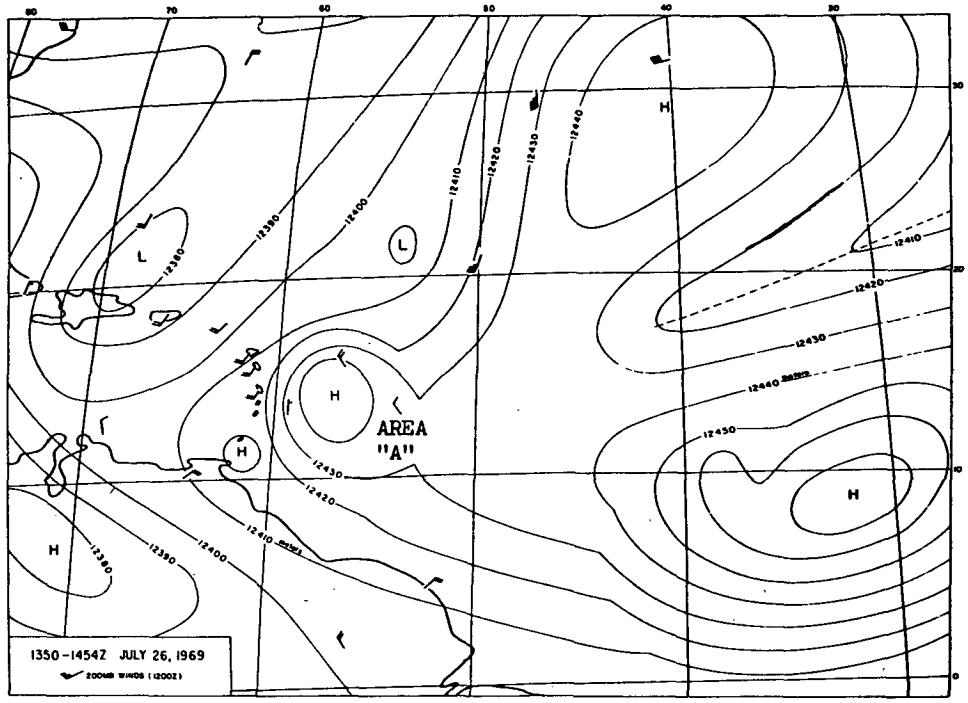

FIG. 5. 200 mb contour analysis for 26 July 1969 (1350–1454 GMT) from the calculated high-cloud velocity field and the observed wind data at 1200 GMT for the area covered by both anvils A and B. Contour spacing is 10 m. (From Chang, 1974.)

The solution has the following implicit form:

$$\gamma t=\log\frac{\left[\frac{D}{\beta}+\eta(r\pm C)\frac{\beta}{\gamma}+\frac{\gamma}{\beta}\right]\left[\frac{D_0}{\beta}-\eta_0(r\pm C)\frac{\beta}{\gamma}-\frac{\gamma}{\beta}\right]}{\left[\frac{D}{\beta}-\eta(r\pm C)\frac{\beta}{\gamma}-\frac{\gamma}{\beta}\right]\left[\frac{D_0}{\beta}+\eta_0(r\pm C)\frac{\beta}{\gamma}+\frac{\gamma}{\beta}\right]}. \quad (15)$$

The upper/lower sign is chosen if η_0, D_0 is a point in curve II/I in Fig. 1.

Figs. 3 and 4 display the time behavior of η and D given by this solution compared with Chang's data. The adjustment time scale is about 3 h in all cases and the initial vorticity is seen to have little impact on the transient evolution of the divergence or upon the value of the vorticity after a few hours. The model computations using Chang's initial data (solid line) agree well with the observed evolution of η and D except that the observed divergence damps faster in time than predicted. The discrepancies between the observed and modelled divergence evolution may be due to the fact that γ is estimated from conditions during the active initial stages and a smaller value may be more appropriate for the present comparison, which covers the evolution almost up to the dissipative stage.

These results suggest that thunderstorms and mesoscales convective disturbances have upper level vorticity and divergence patterns that adjust toward quasi-equilibrium on time scales of tens of minutes and a few hours, respectively. The important agent in the generation of this divergence seems to be the local pressure pattern. The outward acceleration of rotation [η^2 term in (1)] appears to be of secondary importance in these two data studies.

4. Application to synoptic scales

The collective influence of cumulus convection on larger scales must be parameterized in synoptic scale investigations. The discussion of the previous section raises the question of appropriate averaging of the individual anvil outflows in synoptic scale convective systems. For the second example of the previous section, a crude estimate of the divergence can be given by the value of γ which is computed on a 300 km grid. For larger scales it may therefore be appropriate to use an area weighted average γ approximated by the value of γ computed from the synoptic scale system itself. This is also justified considering the high frequency with which synoptic supergradient pressure patterns coincide with observed outflow regions (Paegle and Paegle, 1976; MacDonald, 1976).

For such large scales the only physically meaningful transient states are those associated with non-negative absolute vorticity. The transient solutions can be most easily obtained for the case of circular pressure patterns.

For weak initial deformation the transient solution is given by (15). Such solutions for a particular initial

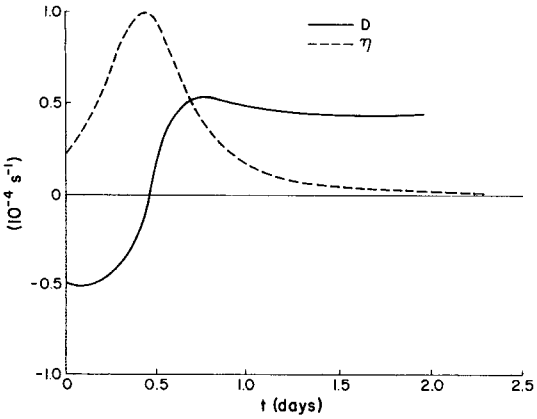

FIG. 6. Time evolution of divergence and absolute vorticity for $\gamma=4\times10^{-5}$ s^{-1}, $D_0=-5\times10^{-5}$ s^{-1}; $\eta_0=2\times10^{-5}$ s^{-1}, $\beta^2=0.75$ for the case of weak initial deformation corresponding to an integral curve like II in Fig. 1.

state are shown in Fig. 6. The value of γ corresponds to a frequently observed supergradient intensity in the subtropics (Paegle and Paegle, 1976).

For the case of strong initial deformation the transient solution is given by (see Appendix)

$$\gamma t=\log\frac{\left[\frac{\gamma}{\beta}+\left(\eta+\frac{D}{\beta}\right)\right]\left[\frac{\gamma}{\beta}-\left(\eta_0+\frac{D_0}{\beta}\right)\right]}{\left[\frac{\gamma}{\beta}-\left(\eta+\frac{D}{B}\right)\right]\left[\frac{\gamma}{\beta}+\left(\eta_0+\frac{D_0}{\beta}\right)\right]}. \quad (16)$$

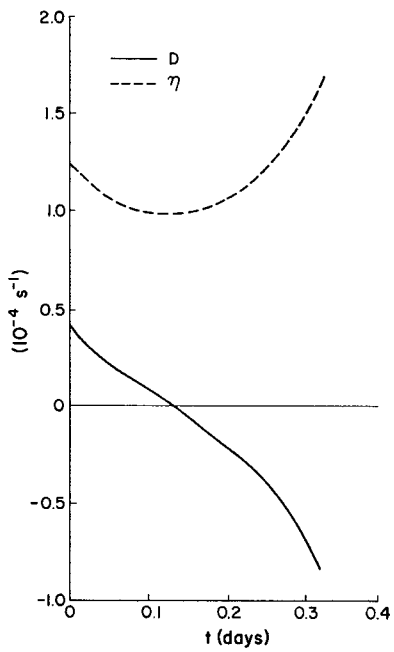

FIG. 7. Time evolution of divergence and absolute vorticity for $\gamma=4\times10^{-5}$ s^{-1}, $\beta^2=0.75$, $D_0=4\times10^{-5}$ s^{-1}, $\eta_0=1.21\times10^{-4}$ s^{-1}, for the case of strong initial deformation corresponding to an integral curve like I in Fig. 2.

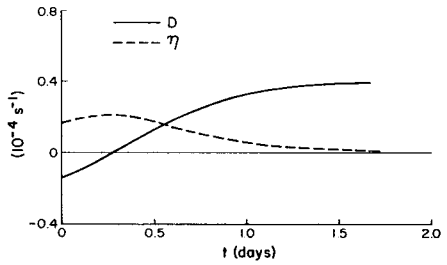

FIG. 8. As in Fig. 6 except for $D_0=-1.33\times10^{-5}$ s^{-1} and $\eta_0=1.82\times10^{-5}$ s^{-1} for an integral curve like II in Fig. 2.

The time evolutions of η and D for selected initial states are displayed in Figs. 7 through 11, corresponding to initial conditions that lie on curves I through V (Fig. 2), respectively. The stable cases converge toward the steady state solutions within about one day. The unstable cases rapidly generate strong convergence and rotation. However, they require strong initial rotation or strong convergence to be realized, and are not likely initial states for the synoptic scales.

These results have particular implications for the upper tropical troposphere, where persistent supergradient pressure systems are often analyzed. The possibility that this is an important component of Hadley circulations and east–west overturnings is therefore a reasonable hypothesis.

5. Conclusions

We have presented the hypothesis that upper tropospheric supergradient pressure patterns may be important to the dynamics of large scale atmospheric divergence fields. This idea was also proposed in an earlier work (Paegle and Paegle, 1976). However, that data investigation left two important questions unanswered. The first, concerning realizability of the divergent supergradient flows, has been addressed in the present article. The other question, concerning data realiability, may be answered in the near future with the FGGE and DST data.

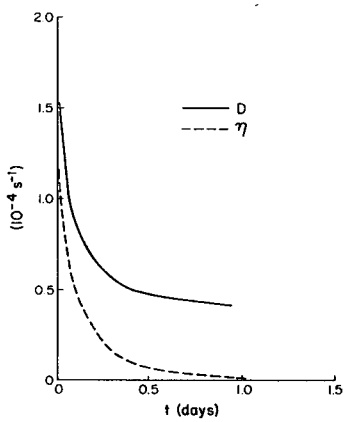

FIG. 9. As in Fig. 6 except for $D_0=1.53\times10^{-4}$ s^{-1} and $\eta_0=1.21\times10^{-4}$ s^{-1} for an integral curve like III in Fig. 2.

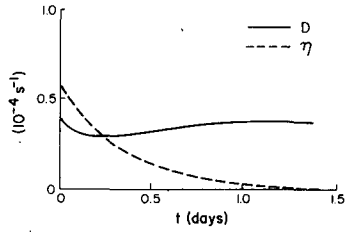

FIG. 10. As in Fig. 6 except for $D_0=4\times10^{-5}$ s^{-1} and $\eta_0=6\times10^{-5}$ s^{-1} for an integral curve like IV in Fig. 2.

The major assumptions of the present approach are the neglect of thermodynamics; neglect of tilting terms in (1) through (4), and the assumption of constant $\nabla^2\phi$, A_g and B_g. Since parcel trajectories do not move into regions of significantly different $\nabla^2\phi$, A_g and B_g in the course of flow adjustment, the last assumption may be reasonable. Tilting terms are not important for synoptic scales and they appeared to be secondary even in Fankhauser's (1974) squall line case. The omission of thermodynamics in our analysis implies neutral stratification. This may be the most restrictive assumption, but a more careful treatment would require cumulus parameterization. This would complicate the analysis greatly. It is relevant to mention that convective clusters are apparently embedded in atmospheres that are quasi-neutral for moist convection (Arakawa and Schubert, 1974).

The question of whether large amounts of internal friction or supergradient pressure fields need to be reproduced in weather prediction models is of practical importance. Although both mechanisms can be used to simulate collective outflows from cumulonimbus towers, their influence on model energetics is very different. The supergradient divergence field generates kinetic energy directly through flow down the pressure gradient. The frictionally produced divergence fields dissipate kinetic energy. Careful data studies are required to estimate the degree to which each process contributes to quasi-steady subtropical and tropical motion fields.

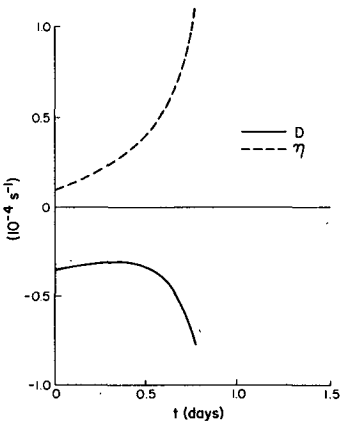

FIG. 11. As in Fig. 6 except for $D_0=-3.5\times10^{-5}$ s^{-1} and $\eta_0=10^{-5}$ s^{-1} for an integral curve like V in Fig. 2.

Acknowledgment. This research was partially sponsored by National Science Foundation, Atmospheric Sciences Section, Grant GA-40387. Part of this research was performed while we were visitors at the National Center for Atmospheric Research, which is funded by the National Science Foundation.

APPENDIX

Time Dependent Solutions

(i) *Weak initial deformation*

Time-dependent solutions to Eqs. (5) and (6) for the case of weak initial deformation can be obtained introducing new variables in such away that

$$\left.\begin{aligned} D&=\beta r\sin\theta\\ \eta\pm C&=r\cos\theta\end{aligned}\right\}, \tag{A1}$$

where the $\pm$ sign depends on the initial conditions.

Then (5) and (6) can be combined to obtain

$$\left.\begin{aligned} \frac{d\theta}{dt}&=\beta r\cos\theta\mp\beta C\\ \frac{dr}{dt}&=0\end{aligned}\right\}. \tag{A2}$$

The last expression holds since $r=$ constant for any integral curve.

Eq. (A2) can now be integrated as

$$\int\frac{d\theta}{r\cos\theta\mp C}=-\frac{\beta}{\gamma}\log\frac{\left[\frac{\gamma}{\beta}\tan\frac{\theta}{2}+(r\mp C)\right]}{\left[\frac{\gamma}{\beta}\tan\frac{\theta}{2}-(r\mp C)\right]}$$

$$+\text{constant}=\beta t, \tag{A3}$$

where the condition $r^2-C^2=\gamma^2/\beta^2$ has been applied. From (A1) it follows that

$$\tan\frac{\theta}{2}=\frac{D}{\beta(r\pm C+\eta)}. \tag{A4}$$

Substitution of (A4) into (A3) gives

$$\gamma t=\log\frac{\left[\frac{\gamma}{\beta^2}D+(r\mp C)(r\pm C+\eta)\right]}{\left[\frac{\gamma}{\beta^2}D-(r\mp C)(r\pm C+\eta)\right]}\times\frac{\left[\frac{\gamma}{\beta^2}D_0-(r\mp C)(r\pm C+\eta_0)\right]}{\left[\frac{\gamma}{\beta^2}D_0+(r\mp C)(r\pm C+\eta_0)\right]}, \tag{A5}$$

where the subscript 0 denotes the initial values used to determine the integration constant.

It can be easily verified that (A5) is identical to (15).

(ii) Strong initial deformation

The transient behavior for this case is obtained introducing new variables as in the previous case, except that hyperbolic functions are used instead of circular functions as in (A1).

REFERENCES

Arakawa, A., and W. Schubert, 1974: Interaction of a cumulus cloud ensemble with the large scale environment. Part I. *J. Atmos. Sci.*, **31**, 674–701.

Blumen, W., 1972: Geostrophic adjustment. *Rev. Geophys. Space Phys.*, **10**, 485–528.

Chang, Y-M., 1974: Analysis of anvil growth from ATS pictures. SMRP Research Paper #122, Dept. of Geophysical Sciences. The University of Chicago. [Available Dept. of Geophysical Sciences, the University of Chicago.]

Davies, T. V., and E. M. James, 1966: *Nonlinear Differential Equations*. Addison-Wesley, p. 26.

Ellsaesser, H. W., 1968: Comparative tests of wind laws for numerical weather prediction. *Mon. Wea. Rev.*, **96**, 277–285.

Fankhauser, J. C., 1974: The derivation of consistent fields of wind and geopotential height from mesoscale rawinsonde data. *J. Appl. Meteor.*, **13**, 637–646.

Greenspan, H. P., 1968: *The Theory of Rotating Fluids*. Cambridge University Press, p. 133.

Holton, J. R., and D. E. Colton, 1972: A diagnostic study of the vorticity balance at 200 mb in the tropics during the northern summer. *J. Atmos. Sci.*, **30**, 1287–1302.

Krishnamurti, T. N., 1971: Observational study of the tropical upper tropospheric motion field during the Northern Hemisphere summer. *J. Appl. Meteor.*, **10**, 1066–1096.

Lindzen, R. S., 1974: Wave-CISK in the tropics. *J. Atmos. Sci.*, **31**, 156–179.

MacDonald, A. E., 1976: On strongly divergent flows of the upper troposphere. Submitted to *Mon. Wea. Rev.*

Paegle, J., and J. N. Paegle, 1974: An efficient and accurate approximation to the balance wind with application to non-elliptic data. *Mon. Wea. Rev.*, **102**, 838–846.

——, and ——, 1976: On geopotential data and ellipticity of the balance equation: a data study. *Mon. Wea. Rev.*, **104**, 1277–1286.

Sadler, J. C., 1975: The upper tropospheric circulation over the global tropics. Hawaii Institute of Geophysics, University of Hawaii, UH MET-75-05, 35 pp. [Available from author, Dept. of Meteorology, University of Hawaii.]